Low Spring Constant Regulates P-Selectin-PSGL-1 Bond Rupture

Yan Zhang, Ganyun Sun, Shouqin Lü, Ning Li, and Mian Long

National Microgravity Laboratory and Center for Biomechanics and Bioengineering, Institute of Mechanics, Chinese Academy of Sciences, Beijing 100190, China

ABSTRACT   Forced dissociation of selectin-ligand bonds is crucial to such biological processes as leukocyte recruitment, thrombosis formation, and tumor metastasis. Although the bond rupture has been well known at high loading rate r_f ($\geq 10^2$ pN/s), defined as the product of spring constant k and retract velocity v, how the low r_f ($<10^2$ pN/s) or the low k regulates the bond dissociation remains unclear. Here an optical trap assay was used to quantify the bond rupture at $r_f \leq 20$ pN/s with low k ($\sim 10^{-3}$–10^{-2} pN/nm) when P-selectin and P-selectin glycoprotein ligand 1 (PSGL-1) were respectively coupled onto two glass microbeads. Our data indicated that the bond rupture force f retained the similar values when r_f increased up to 20 pN/s. It was also found that f varied with different combinations of k and v even at the same r_f. The most probable force, f^*, was enhanced with the spring constant when $k < 47.0 \times 10^{-3}$ pN/nm, indicating that the bond dissociation at low r_f was spring constant dependent and that bond rupture force depended on both the loading rate and the mechanical compliance of force transducer. These results provide new insights into understanding the P-selectin glycoprotein ligand 1 bond dissociation at low r_f or k.

INTRODUCTION

Selectin-ligand interactions mediate the tethering and rolling of circulating cells on endothelium, an initiating event of the multistep adhesion and signaling process in inflammatory responses and tumor metastases (1–6). There are three known members of the selectin family—P-, E-, and L-selectin—which consists of an N-terminal, C-type lectin domain (L), followed by an epidermal growth factor-like module (E), multiple copies of consensus repeat (CR) units characteristic of complement binding proteins, a transmembrane segment, and a short cytoplasmic domain (7,8). P-selectin is expressed on activated endothelial cells and platelets and interacts with P-selectin glycoprotein ligand 1 (PSGL-1) expressed on microvillus tips of leukocytes (9,10). Formation and dissociation of P-selectin-PSGL-1 bonds under blood flow are crucial to understand the biophysical bases of receptor-ligand interactions in regulating cell adhesions.

When an external force is introduced, the work done by force is assumed to tilt the energy barrier of the receptor-ligand complex and to accelerate the rupture of the receptor-ligand bond (11). Forced bond rupture is regulated by the loading rate of force, r_f, or the product of the spring constant of force transducer, k, and retract velocity, v, that is, $r_f = k \times v$. For example, rupture force f for dissociating P-selectin-PSGL-1 bond is found to exhibit two stepwise linear regimes against $\log(r_f)$ when a constant r_f is applied (12–17) but to reduce into a single regime when a jump/ramp mode of applied force is introduced (12). Bond rupture is also regulated by such biophysical factors as force history, contact duration, and approach velocity. For example, discrepancies existing between the force dependence of reverse rates for P-selectin-PSGL-1 interactions, derived from the two types of bond lifetime and unbinding force measurements, have been attributed to different force histories on of the bond (16). The rupture force of P-selectin-PSGL-1 bonds exhibits a transition phase when it increases with contact duration followed by an equilibrium phase when it reaches a plateau, whereas it increases with a logarithm of approaching velocity only if the velocity is beyond a threshold ($\sim 10^4$ nm/s) (15). Thus, it is important to understand the underlying mechanism that regulates the rupture of the P-selectin-PSGL-1 bond at different biophysical factors.

Bond dissociation under applied forces has been extensively investigated using such biophysical approaches as atomic force microscopy (AFM) (13–16,18,19), biomembrane force probe (BFP) (12,20), microcantilever (21), flow chamber (18,22), and optical trap (OT) (17,23). In a typical measurement, a receptor-coupled surface is forced to approach, interact with, and retract from a ligand-immobilized surface, and the bond rupture force, f, is measured at a given r_f. To the best of our knowledge, six studies have been conducted to quantify the rupture forces of P-selectin-PSGL-1 bonds using AFM, BFP, and OT assays in different labs (12–17) where r_f is varied 10^1–10^5 pN/s (Table 1). It should be pointed out that there exist the differences in the length of interacting molecules (LE+2CR, LE+6CR, LE+9CR, or LE+9CR+Fc constructs, soluble or membrane PSGL-1), the variations in length and elasticity of linker molecules (antibodies-antigen, biotin-(strep)avidin, or covalent linkers), and the distinctive schemes of molecular immobilization (physisorption via antibodies, covalent immobilization via antibodies, or biotin-(strep)avidin immobilization in a lipid layer) onto a sharp or round surface (12–17), which affects significantly the bond dissociation kinetics (k_r^0 and χ_β) (Table 1).

TABLE 1 Summaries of bond dissociation of P-selectin-PSGL-1 interactions measured in different labs using various techniques

P-Selectin* (length)	PSGL-1* (length)	Molecular Linkage	Assay (probe geometry)	r_f, 10^3 pN/s	k, pN/nm	v, nm/s	$f*$, pN	k_r^0 s^{-1}	χ_β, nm	Ref.
LE+6CR+Fc (31 nm)	mPSGL-1 (53 nm)	immobilized via biotin-avidin	AFM (sharp)	12.8–256	64	200–4500	120–165	0.02	0.25	(13)
LE+9CR+Fc (43 nm)	mPSGL-1 (53 nm)	immobilized via mAbs	AFM (sharp)	0.1–10	10–40	2000–25,000	80–250	0.20	0.14	(14)
LE+9CR (40 nm)	sPSGL-1 (50 nm)	immobilized via biotin-avidin	BFP (round)	0.3–30	0.2–2	17–1400	70–150	0.37	0.23	(12)
LE+2CR+Fc (15 nm)	mPSGL-1 (53 nm)	covalently immobilized via carbodimide	OT (round)	0.025–0.6	0.004–0.05	500–12,000	2.5–50	4.30	0.14	(17)
LE+9CR (40 nm)	sPSGL-1 (50 nm)	physisorbed via mAbs and immobilized in a lipid layer	AFM (sharp)	10^{-2}–10^2	4–13	30–30,000	10–150	0.08 33.6	2.41 0.10	(16)
LE+9CR (40 nm)	mPSGL-1 (53 nm)	physisorbed via mAbs and immobilized in a lipid layer	AFM (sharp)	0.13–45.6	5–38	100–34,900	25~200	0.91 48.7	0.72 0.07	(15)
LE+9CR (40 nm)	mPSGL-1 (53 nm)	physisorbed via mAbs	OT (round)	0.021~0.188	0.0107–0.047	500–4000	9.3–37.8	0.37	0.49	this study
LE+9CR (40 nm)	mPSGL-1 (53 nm)	physisorbed via mAbs	OT (round)	0.001~0.020	0.0025–0.0075	500–4000	2.2–5.8	N/D	N/D	this study

*Molecular length was estimated from Ushiyama et al. (8) and Li et al. (9) by setting 4, 4, 3, and 3 nm for LE, CR, Fc, and lipid bilayer, respectively.

Thus, it is necessary to further understand how the loading rate itself and even the entire loading history (spring constant k and retract velocity v) regulate the bond rupture (16,19). Moreover, few reports of rupture forces measured at low r_f ($<10^2$ pN/s) have been found. To complete the rupture force versus loading rate profile, bond dissociation measurements at low loading rates are required by either reducing the spring constant or lowering the retract velocity. Considering the technical difficulties in lowering indefinitely the velocity when visualizing bond dissociation, we used here an OT assay, applying a low spring constant 10^{-3}–10^{-2} pN/nm to measure the rupture force spectrum of P-selectin-PSGL-1 bonds at low r_f.

Another important point found in the literature (12–17) is that the rupture forces so measured are different even at the same or similar loading rates where r_f is varied in the range 10^1–10^5 pN/s with a combination of k in the range 10^{-3}–10^1 pN/nm and v in the range 10^1–10^4 nm/s (Table 1), suggesting that the force transducer stiffness or the retract velocity separately regulates the dissociation of receptor-ligand bonds. Spring constants of interacting molecules and the force transducer cooperatively contribute to bond dissociation measurements where the two springs are linked in series in a typical AFM, BFP, or OT measurement. For example, the high effective spring constant enhanced the rupture force of the biotin-streptavidin bond, presumably by perturbing the energy landscape and affecting the apparent rupture forces via a sufficiently stiff force transducer (19). Noting that the spring constant reported was higher than or close to those for interacting molecules themselves ($\sim$1–10 pN/nm), these data suggest that the stiffness of interacting molecules plays a dominant role in bond rupture. The force transducer stiffness, however, would manipulate the bond rupture differently when it is much lower than those for interacting molecules, which has been poorly understood. In the OT assay here, we employed a very soft force transducer ($k \sim 10^{-3}$–10^{-2} pN/nm) to isolate the effects of the spring constant (and retract velocity) on the bond rupture of P-selectin-PSGL-1 interactions. Our data indicated that the bond dissociation was spring constant dependent at low r_f.

MATERIALS AND METHODS

Proteins and antibodies

PSGL-1 was purified from human neutrophils following a modified protocol, and the purity of the proteins was analyzed by sodium dodecylsulfate-polyacrylamide gel electrophoresis on 7.5% polyacrylamide gels followed by silver staining (15). Soluble P-selectin consisting of lectin-epithelial growth factor domains plus nine CRs but no transmembrane and cytoplasmic domains (8), anti-P-selectin capturing (S12) and blocking (G1) monoclonal antibodies (mAbs) (24), and anti-PSGL-1 capturing (PL2) and blocking (PL1) mAbs (25) were generous gifts from Dr. Rodger P. McEver (Oklahoma Medical Research Foundation). Bovine serum albumin (BSA) was purchased from Sigma Chemical (St Louis, MO).

Functionalized microbeads

We incubated 2.32-μm- and 5.66-μm-diameter silicon microbeads (Bangs Lab, Fishers, IN) overnight at 4°C in 10 μg/ml of capturing mAbs S12 and PL2, respectively. The microbeads were washed twice with phosphate buffer solution and incubated in 2% BSA to block nonspecific adhesions for 12 h. Capturing the efficiency of protein was examined by flow cytometry, using CD58, which is constitutively expressed on red blood cells at a known density as a standard (26,27). S12- and PL2-captured microbeads were then incubated with 15 ng/ml P-selectin and PSGL-1 for 12 h, respectively. After rinsing with phosphate buffer solution and being reblocked with BSA, P-selectin- and PSGL-1-coupled microbeads were ready for measurements.

Site densities of surface proteins coated on microbeads were determined using flow cytometry and immunoradiometric assay as described previously (26,27). Two calibration curves for coupled P-selectin and PSGL-1 proteins were obtained by plotting the protein site density against the mean fluorescence intensity of the capturing mAb (27), thereby allowing the calculation

of the site densities of the protein of interest from the mean fluorescence intensities of the capturing mAbs. To obtain the infrequent binding events mediated by the single P-selectin-PSGL-1 bond, the site densities of both proteins were adjusted to reach the low adhesion probability <25%.

Optical trap set-up

A commercial OT Combisystem (Carl Zeiss, Munich, Germany) (Fig. 1 A) was modified to visualize the dissociation of P-selectin-PSGL-1 bonds. Here OT is constructed on a Zeiss Axiovert 200 inverted microscope. A diode-pumped yttrium aluminum garnet laser (Compass 1064, Coherent, Santa Clara, CA) with the maximum power of 4 W coupled with an optical fiber was focused with a $100\times$ oil objective (UplanFL, Carl Zeiss) with a numerical aperture of 1.30 to form an unmovable OT. The microscope stage was replaced by a high-speed XYZ piezo nanopositioner and scanner (P-733.3DD, Physik Instrumente, Karlsruhe, Germany) with a digitalized piezo controller (E-710, Physik Instrumente). The immobilized microbead was forced to move with the piezo stage, and the approach velocity, contact duration, and retract velocity were controlled using a custom user interface. Real time images of microbead movement were recorded by a charge-coupled device camera (HV-D30, Hitachi, Tokyo, Japan) with a spatial and temporal resolution of 125 nm/pixel and 40 ms/frame for offline analysis. A cross correlation method described previously (28) was used to determine the off-center displacement of the P-selectin-coupled microbead from the trap center with an accuracy of $\sim$2 nm along the x and y axes. The spring constant of the trap was determined using the Stokes law (29), which spans from 2.5×10^{-3} to 47.0×10^{-3} pN/nm upon varied laser power for mimicking the compliant nature of microvillus (30). All the measurements were done at room temperature (261°C $\pm$ 1°C).

Bond rupture assay

Measurements of bond rupture were performed in a custom-made glass sample cell ($\sim$14 $\times$ 10 $\times$ 0.5 cm). Each of 10^3 P-selectin- and PSGL-1-coupled microbeads was injected separately into the sample cell. The 5.66-μm-diameter microbeads coupled with PSGL-1 settled down quickly and adhered stably onto the coverslip surface. Once a floating 2.32-μm-diameter microbead coupled with P-selectin was trapped by the OT, an immobilized PSGL-1-coupled microbead was brought by the piezo stage to make contact with the trapped P-selectin-coupled microbead at a given contact duration of 2 s (Fig. 1 B). The adhesion at the endpoint of the contact period was observed microscopically from bouncing the off-center P-selectin-coupled microbead back to the center of the trap upon retracting it away from the immobilized PSGL-1-coupled microbead (Fig. 1 C). This approach-contact-retract cycle was repeated >250 times per pair to collect the data of rupture forces from bond-formed events (Fig. 1 C). Here, the bond rupture force, f, was determined by the product of the off-center displacement, d, and the spring constant of the trap, k. Twenty-five loading rates with a systematically varied spring constant and retract velocity were used for rupture force measurements (Tables 2 and 3), and 27–80 rupture forces were obtained for each loading rate. In the case of the specificity measurement, an alternative loading rate was used.

Mechanokinetic theory and data analysis

Data for bond dissociation were analyzed using a first-order irreversible unbinding kinetics,

$$P_{b}(t) = \exp\left[-\int_{0}^{t} k_{r}'(t)dt'\right], \qquad (1a)$$

and

$$P_{b}(0) = 1, \qquad (1b)$$

where $P_{b}(t)$ is the probability of having a bond at time 0 to remain bound at time t, and $k_{r}(t)$ is the reverse rate of a bond at time t. Along a
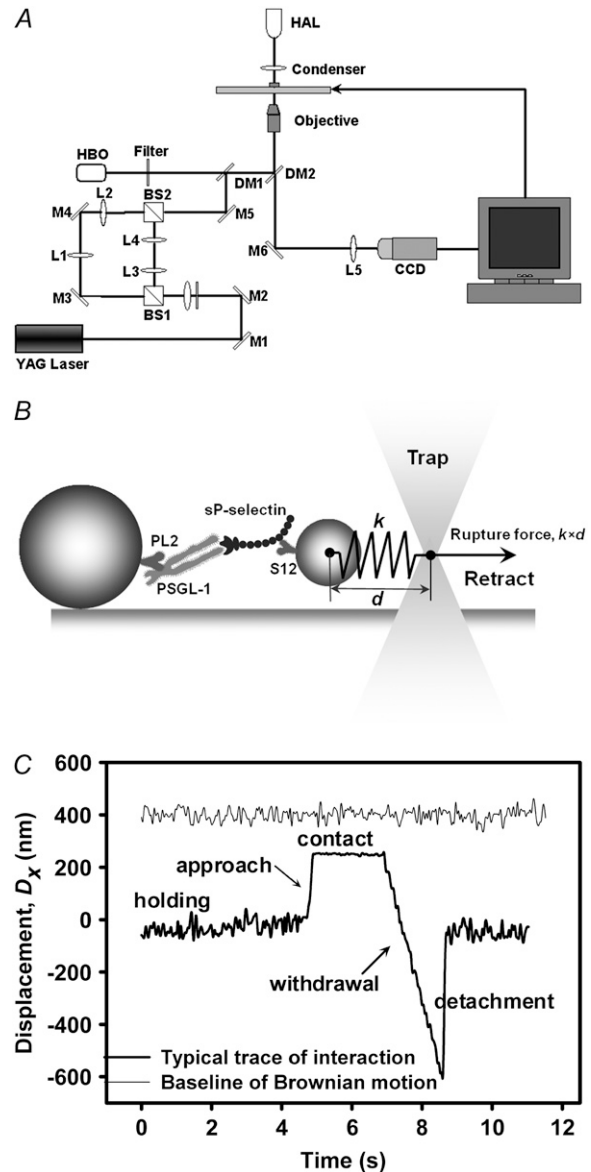

FIGURE 1 OT set-up and experimental procedure. (A) Schematic of an OT system. M, Mirror; BS. Beam splitter; L, Lens; DM, Dichroic mirror. (B) Illustration of functionally coated molecule pair. P-selectin was coupled via precoated capturing mAb S12 onto a 2.32-μm-diameter microbead, and PSGL-1 was coupled via precoated capturing mAb PL2 onto a 5.66-μm-diameter microbead. P-selectin-coupled microbead was held in a trap and brought into contact with a PSGL-1-coupled microbead to form a selectin-ligand bond. Bond rupture was visualized by a sudden bounce of the off-center microbead back to the center of the trap. (C) Typical time course of off-center displacement for rupturing the P-selectin-PSGL-1 bond at $k = 0.0025$ pN/nm and $v = 500$ nm/s (thick line). The P-selectin-coupled microbead was driven to approach, contact, and retract from the PSGL-1-coupled microbead and was bounced back to trap center when the bond dissociated. Also included is the baseline of microbead displacement without bond formation (thin line; moved upward away from the origin for the sake of clarity). The noise represents the Brownian motion of the trapped microbead.

constant loading rate (r_{f}) force history $f = r_{f} \times t$, the time dependence of $P_{b}(t)$ and $k_{r}(t)$ can be transformed to their respective force dependences in both forms of cumulative probability $P_{c}(f)$ and probability density $P_{d}(f)$ (16),

TABLE 2 Summaries of estimated kinetic parameters of P-selectin-PSGL-1 bonds at given loading rates with combined spring constants and retract velocities

r_f (pN/s)	k (10^{-3} pN/nm)	v (nm/s)	k_r^0 (s^{-1})*	χ_β (Å)*	R^2
10	2.5	4000	0.61	40.1	0.78
	3.4	2982	0.22	46.7	0.83
	5.0	2000	0.50	18.3	0.98
	10.7	936	0.16	11.3	0.93
	20.0	500	0.25	4.7	0.75
15	3.8	4000	0.31	57.1	0.93
	5.9	2982	0.11	41.7	0.94
	7.5	2000	0.48	16.1	0.81
	16.0	936	0.22	7.2	0.88
	30.0	500	0.17	4.2	0.83

*Kinetic parameters were obtained by fitting an individual rupture force histogram using Eq. 2 together with Eq. 3.

$$P_c(f) = 1 - \exp\left[-r_f^{-1}\int_0^t k_r'(f)dt'\right], \quad (2a)$$

and

$$P_d(f) = r_f^{-1}k_r(f)\exp\left[-r_f^{-1}\int_0^t k_r'(f)dt'\right], \quad (2b)$$

which correspond, respectively, to cumulative frequency and histogram of rupture forces.

An explicit Bell model (11) in which the reverse rate is assumed to depend exponentially on applied force is used,

$$k_r(f) = k_r^0\exp(\chi_\beta f/k_B T), \quad (3)$$

where k_r^0 is the zero-force reverse rate, k_B is the Boltzmann constant, T is the absolute temperature, and χ_β is a measure of bond compliance width. Since external force is unable to be applied instantaneously in experimental measurements, bond dissociation depends on time t through force f. The most probable rupture force, f^*, follows the so-called dynamic force spectroscopy (DFS) theory (20,21,31,32):

TABLE 3 Summaries of estimated kinetic parameters of P-selectin-PSGL-1 bonds at systematically varied spring constants and retract velocities

v (nm/s)	k (10^{-3} pN/nm)	k_r^0 (s^{-1})*	χ_β (Å)*	R^2
500	2.5/5.0/20.0/30.0/47.0	0.17	6.3	0.94
936	2.5/5.0/10.7/16.0/47.0	0.30	5.5	0.96
2000	2.5/3.4/5.0/7.5/10.7/20.0/47.0	0.68	5.3	0.88
2982	2.5/3.4/5.0/47.0	0.66	3.5	0.98
4000	2.5/3.8/5.0/47.0	0.85	3.2	0.97

k (10^{-3} pN/nm)	v (nm/s)	k_r^0 (s^{-1})	χ_β (Å)	R^2
2.5	500/936/2000/2982/4000	N/D	N/D	N/D
3.4	2000/2982	N/D	N/D	N/D
5.0	500/936/2000/2982/4000	N/D	N/D	N/D
10.7	936/2000	N/D	N/D	N/D
20.0	500/2000	N/D	N/D	N/D
47.0	500/936/2000/2982/4000	0.31	4.8	0.92

*Kinetic parameters were obtained by fitting an f^* versus log(r_f) profile using Eq. 4.

$$f^* = \frac{k_B T}{\chi_\beta}[\ln(k) + \ln(v)] - \frac{k_B T}{\chi_\beta}\ln\left(\frac{k_r^0 k_B T}{\chi_\beta}\right). \quad (4)$$

Two line segments in the f^* versus $\ln(r_f)$ plot are interpreted as two Bell models in the series,

$$(k_r)^{-1} = \sum_{i=1}^2[k_{ri}^0\exp(\chi_{\beta i}f/k_B T)]^{-1}, \quad (5)$$

which can be fitted by

$$(r_f)^{-1} = \sum_{i=1}^2[(k_{ri}^0 k_B T/\chi_{\beta i})\exp(\chi_\beta f^*/k_B T)]^{-1} \quad (6)$$

to yield two sets of Bell model parameters (k_{ri}^0, $\chi_{\beta i}$) ($i = 1, 2$) (16,31).

RESULTS

Binding was specifically mediated

The adhesion frequency at a sufficiently long contact time ($t = 2$ s) was used to quantify the bindings between P-selectin- and PSGL-1-coupled microbeads. As exemplified in Fig. 2 A, adhesion frequencies measured using OT assay were mediated by specific P-selectin-PSGL-1 interactions, because they were present when the microbeads were coated with S12 and PL2 mAbs to capture P-selectin and PSGL-1 constructs, respectively, but were abolished when P-selectin or PSGL-1 constructs were absent. In addition, binding was blocked by mAbs against PSGL-1 (PL1), P-selectin (G1), and the calcium chelator EDTA. The isolation of specific P-selectin-PSGL-1 binding from nonspecific interactions was further confirmed by comparing their rupture forces. As exemplified in Fig. 2 B, bond rupture forces at a typical loading rate $r_f = 13.7$ pN/s shifted rightward dramatically when both P-selectin and PSGL-1 molecules were present, as compared to those when the two microbeads were coated with BSA. It was also pointed out that ~90% of binding events measured are single-bond events when the site densities of interacting molecules were adjusted to have the adhesion frequency of <20% (Fig. 2 A) (26,27,33–35). Taken together, the bindings between two microbeads were specifically mediated, most likely, by a single binding event of P-selectin and PSGL-1 pair.

Rupture force retained the same with increased loading rates at a low spring constant

We first examined the bond dissociation at $r_f \lesssim 20$ pN/s. Here r_f was systematically varied by changing the retract velocity at a given spring constant. Bond rupture forces so measured distributed similarly with varied r_f at $k = 2.5 \times 10^{-3}$ (Fig. 3 A) or 5.0×10^{-3} (Fig. 3 B) pN/nm, suggesting the loading rate independence of rupture force at low r_f. This was further confirmed when plotting the most probable force against loading rate (Fig. 3 C). Here f^* yielded the same values of 2.2–2.6 and 3.9–4.6 pN when r_f varied in the ranges 1.3–10 and
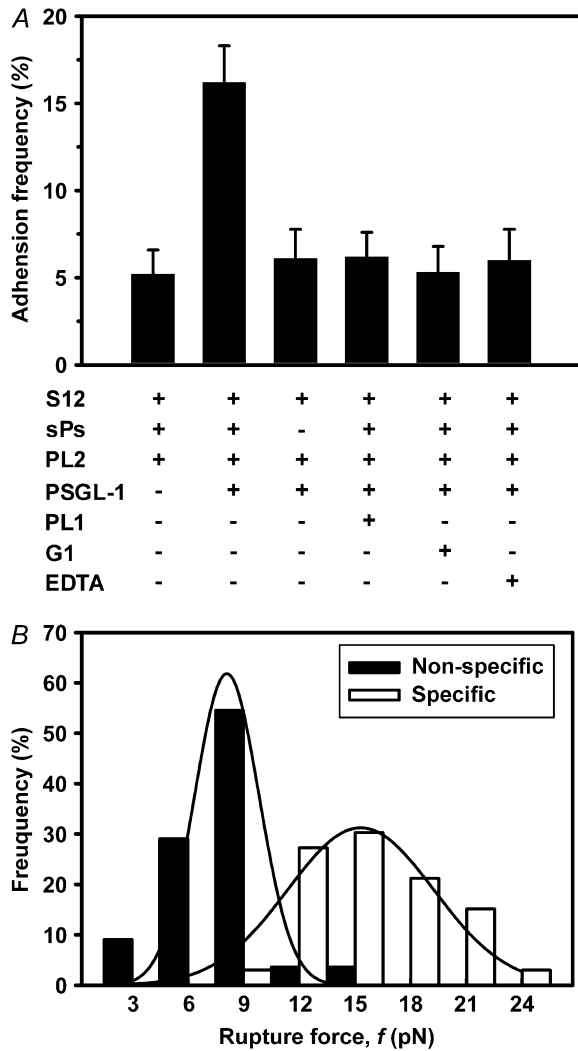
FIGURE 2 Binding specificity. (*A*) Adhesion frequency was obtained from 10 pairs of P-selectin- and PSGL-1-coated microbeads with 100 contacts for each pair at a contact duration of 2 s. Data were presented as the mean ± SD. (*B*) Rupture force was obtained from six pairs of P-selectin- and PSGL-1-coated microbeads with 100 contacts for each pair at a loading rate $r_f = 13.7$ pN/s.

FIGURE 3 Bond dissociation at low loading rates. (*A* and *B*) Dependence of rupture force distribution on loading rates at the same spring constant of $k = 2.5 \times 10^{-3}$ (*A*) and 5.0×10^{-3} (*B*) pN/nm. Histograms of rupture forces measured were plotted against the loading rates of $r_f = 1.25$–10 (*A*) and $r_f = 2.5$–20 (*B*) pN/s. (*C*) Independence of most probable force, f^*, on loading rates ($r_f \leq 20$ pN/s). Data are presented as the mean ± SD. When not visible, error bars are within the symbol. The solid line represents the average most probable force at that spring constant, and the dashed line illustrates a constant force $f^* = 4.1$ pN estimated from thermal energy.

2.5–20 pN/s, respectively. Similar independences were observed at $k = (3.4, 10.7,$ or $20.0) \times 10^{-3}$ pN/nm even when only two r_f values were used at each k. Interestingly, f^* so measured at $k < 10 \times 10^{-3}$ pN/nm seems to be comparable to that estimated from thermal activation where force stemming from the energetic barrier of thermal activation yields 4.1 pN when the thermal energy is $k_B T = 4.1$ pN·nm, and the reactive compliance is ~1 nm (36) (*dashed line* in Fig. 3 *C*). To the best of our knowledge, this is the first study to unravel the bond dissociation of P-selectin-PSGL-1 interactions at such low loading rates using a very soft OT. These data were different from those described previously at high r_f where f^* increased piecewise with r_f (12–17), implying that bond dissociation might follow distinctive mechanisms at low loading rates with low spring constants.
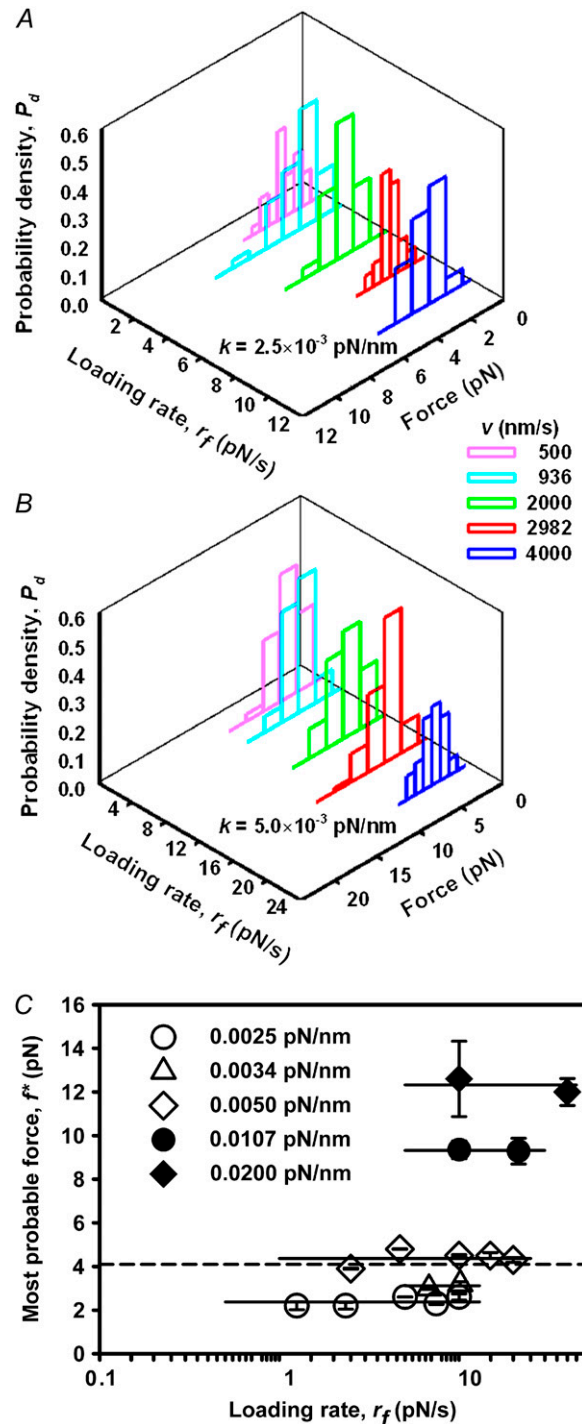
Bond dissociation was different at the same loading rate

To further understand the bond rupture of P-selectin-PSGL-1 interactions at low loading rates, five combinations of spring constants, $k = (2.5, 3.4, 5.0, 10.7,$ and $20.0) \times 10^{-3}$ pN/nm together with respective retract velocities, $v = 4000, 2982, 2000, 936,$ and 500 nm/s were used to retain the same loading rate of 10 pN/s. As exemplified in Fig. 4 A, rupture forces still exhibited a single peak at each combination of spring constant and retract velocity but shifted toward higher force values at the higher spring constants and the corresponding lower retract velocities, indicating that the rupture force is no longer a single-value function of loading rate and that bond dissociation depends on both the spring constant and the retract velocity even at the same loading rate. It was also found that the rupture force distribution was much broader at higher spring constants, implying the stochastic nature of bond dissociation. Similar data were obtained when the loading rate was set to be

the same value of 15 pN/s using varied $k = (3.8, 5.0, 7.5, 16.0,$ and $30.0) \times 10^{-3}$ pN/nm together with respective $v = 4000, 2982, 2000, 936,$ and 500 nm/s (Fig. 4 B). Taken together, these results indicated that no unique rupture force spectrum was obtained at a given loading rate when the spring constant and retract velocity were systematically varied.

We further compared the dissociation kinetics of P-selectin-PSGL-1 bonds using a first-order irreversible unbinding approach. The probability density of rupture force (Fig. 4) was fitted using Eq. 2a, together with the Bell model (Eq. 3), and the estimated kinetic parameters were summarized in Table 2. Here the zero-force reverse rate k_r^0 varied slightly from 0.61 to 0.25 and from 0.31 to 0.17 s^{-1}, but the reactive compliance χ_β was reduced significantly from 40.1 to 4.7 and 57.1 to 4.2 Å at $r_f = 10$ and 15 pN/s, respectively, when k yielded from 2.5 to 20.0×10^{-3} pN/nm at $r_f = 10$ pN/s and from 3.8 to 30.0×10^{-3} pN/nm at $r_f = 15$ pN/s. These estimations further supported the above observations that bond dissociation follows along different pathways at the same loading rate and suggested that bond reactive compliance (χ_β) is altered by mechanical compliance of force transducer.

The spring constant dominated the bond dissociation at low loading rates

To isolate the impact of the spring constant on the forced dissociation of P-selectin-PSGL-1 bonds, k was systematically varied from 2.5×10^{-3} to 47.0×10^{-3} pN/nm at a given retract velocity (as seen in Table 3). The bond rupture was quantified using the most probable force, f^*, obtained from the mean value of the highest force bin of the rupture force histogram at each case (15,20). As exemplified in Fig. 5 A, f^* was enhanced with k at a single retract velocity. More importantly, all f^* values at different retract velocities appeared to fall into a single line, suggesting that the bond dissociation is independent of retract velocity when $k \leq 30.0 \times 10^{-3}$ pN/nm. This was further confirmed by fitting the data using Eq. 4, which returned the kinetic parameters of P-selectin-PSGL-1 interactions, as summarized in Table 3. A fivefold difference in the zero-force reverse rate, k_r^0 ($= 0.17$ and 0.85 s^{-1}, respectively), was found between the lowest (2.5×10^{-3} pN/nm) and highest (47.0×10^{-3} pN/nm) spring constants. By comparison, the reactive compliance, χ_β, varied within a factor of two (6.3 and 3.2 Å, respectively).

To further isolate the impact of retract velocity on bond dissociation, v was systematically varied from 500 to 4000 nm/s at a given spring constant (as seen in Table 3). As exemplified in Fig. 5 B, f^* retained the same values with two to five retract velocities at a single $k = (2.5, 3.4, 5.0, 10.7,$ or $20.0) \times 10^{-3}$ pN/nm but increased with the spring constant at a single v, indicating that bond dissociation is dependent on the spring constant when $v \leq 4000$ nm/s. No best-fit predictions using Eq. 4 could be obtained for f^* versus v data, suggesting that DFS theory was no longer applicable at low spring constants. Exceptionally, f^* was enhanced with v at
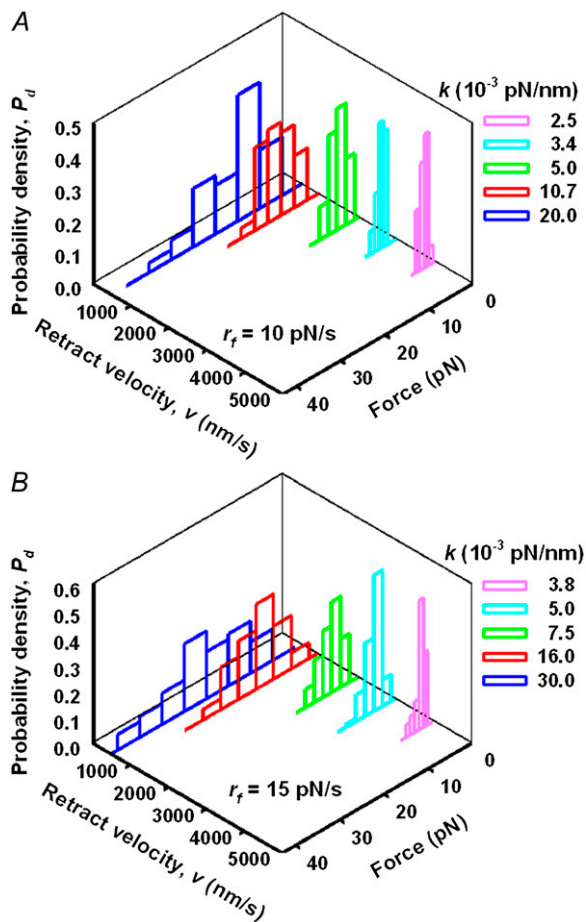

FIGURE 4 Dependence of rupture force distribution on varied spring constants and retract velocities. Histograms of rupture forces measured were plotted against the combined spring constant and retract velocity at the same loading rate of $r_f = 10$ (A) and $r_f = 15$ pN/s (B). Five retract velocities of $v = 500, 936, 2000, 2982,$ and 4000 nm/s were adjusted in rupture force measurements at each loading rate with the corresponding spring constants.

FIGURE 6 Dependence of most probable force on loading rates by plotting f^* against $\log(r_f)$ (*open diamonds*). The line is the prediction using Eq. 4. Also plotted were those data published previously (12–17).
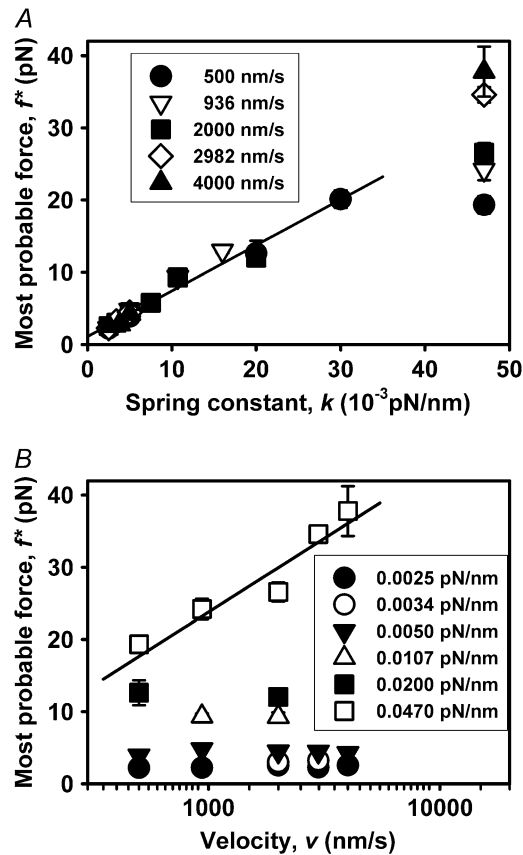
FIGURE 5 Dependence of the most probable force on the spring constant (*A*) and retract velocity (*B*). Data (*points*) were calculated as the peak forces from rupture force histograms. (*A*) f^* was plotted against k at a single retract velocity 500 (*solid circles*), 936 (*open triangles*), 2000 (*solid squares*), 2982 (*open diamonds*), or 4000 (*solid triangles*) nm/s. The line is a trend line. (*B*) f^* was plotted against v at a single spring constant 2.5 (*solid circles*), 3.4 (*open circles*), 5.0 (*solid triangles*), 10.7 (*open triangles*), or 20.0 (*solid squares*) $\times 10^{-3}$ pN/nm. Data are presented as the mean ± SD. When not visible, error bars are within the symbol. f^* was also plotted against v at $k = 47.0 \times 10^{-3}$ pN/nm (*open squares*). The line is the prediction using Eq. 4.

high $k = 47.0 \times 10^{-3}$ pN/nm, and the prediction (*line*) using Eq. 4 was in excellent agreement with the data (*open squares*) (Fig. 5 *B* and Table 3). Taken together, bond dissociation was dominated by the spring constant at low loading rates and the bond rupture force depended on loading rate and mechanical compliance of force transducer.

Bond dissociation followed stepwise regimes at high loading rates

To further examine the dependence of most probable forces at high loading rates, r_f was systematically varied in the range 21–188 pN/nm. As exemplified in Fig. 6, f^* appeared to increase stepwise with $\log(r_f)$. The prediction (*line*) using Eq. 4 was in excellent agreement with the measured data (*open diamonds*). It was also indicated that most probable forces of P-selectin-PSGL-1 bonds measured using the current OT assay were comparable to those obtained using AFM, BFP, and
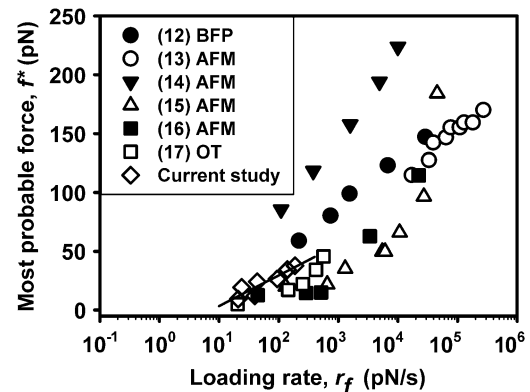
OT assays at $r_f \sim 25$–256,000 pN/nm (12–17). This was further confirmed by comparing the kinetic parameters predicted using Eqs. 4–6 (Table 1), and the kinetic parameters estimated here were consistent with those published previously (12–17).

In addition to loading rate dependence of bond rupture force (rupture force approach) (12–17,20), bond dissociation is also able to be characterized using force dependence of bond lifetime (lifetime approach) (18,22,37). P-selectin-PSGL-1 has been found to behave like a catch bond at applied force $f < 30$ pN and to reach the shortest lifetime <0.3 s at the lowest force measured (18). There might also exist another slip-catch bond transition at applied forces as low as <5 pN when considering the zero-force reverse rate $k_r^0 \sim 1$ s^{-1} (that is, zero-force lifetime ~ 1 s) (26,27,34,35). Our data indicated that the bond lifetime predicted from the rupture force reported here decreased monotonically with force and exhibited the nature of a slip bond (data not shown), presumably due to the discrepancies in estimating the reverse rate between two approaches (16). To unravel the possible slip-catch bond transition, a very soft force transducer is required to measure the force dependence of the bond lifetime at applied forces as low as <5 pN. Caution should be taken since the bond dissociation pathway is different even at the same loading rate and the bond rupture force is spring constant dependent at a low spring constant, as found in this study.

DISCUSSION

The goal of this work is to understand the bond dissociation of P-selectin-PSGL-1 interactions at low loading rates and to elucidate the regulating mechanisms in bond ruptures by systematically varied spring constants and retract velocity. Technically, the state-of-the-art techniques with high spatial and force resolutions are required to conduct the bond dissociation measurements at low loading rates. In this work, we used an OT approach with an accuracy of ~ 2 nm and a spring constant of $\sim 10^{-3}$ pN/nm, which resulted in the force resolution of $\sim 5 \times 10^{-3}$ pN to map weak noncovalent bonds at

as low as $r_f \sim 1$–20 pN/s (Fig. 3 C). It also enables us to conduct the measurements at an intermediate $r_f \sim 20$–200 pN/s (Fig. 6), even though it is hard to further extend r_f to higher content due to technical limitations in applying very high retract velocities at very low spring constants. Thus, the OT approach can quantify the bond dissociation at low spring constants (and then low loading rates) and to establish a complete f^* versus $\log(r_f)$ profile (Figs. 3 C and 6).

We further compared our results with those reported previously when a similar OT set-up was used (17). In the previous study, the loading rate dependence of rupture force was measured for the P- and L-selectin-PSGL-1 complexes at high loading rates of 25–600 pN/s, in which the majority of data was obtained at $r_f > 100$ pN/s. Kinetic parameters (k_r^0 and χ_β) were predicted by fitting the data using the DFS theorem (17). By contrast, a similar bond dissociation was done at low r_f (1–188 pN/s) in this study, in which the majority of data was obtained at $r_f < 100$ pN/s. DFS theory was also applied at $r_f \sim 21$–188 pN/s but no longer available at $r_f \sim 1$–20 pN/s. More importantly, the impact of the spring constant was isolated from that of the loading rate by adjusting the spring constant and retract velocity at the same loading rate. Thus, our results enable us not only to supplement the rupture force versus loading rate profile by extrapolating r_f to low content but also to unravel the nature of the spring constant-dependent bond rupture.

Bond strength depends on how fast external force is applied. When the bond with a stiffness k_m is linked to the tip or substrate with a stiffness k, the effective spring constant k_s for coupling force to the bond is determined by the serial compliance $1/k_s = 1/k_m + 1/k$, which defines the impact of applied force on energy landscape (and, therefore, on k_r^0 and χ_β). When the bond is connected to a stiff probe like an AFM cantilever ($k > 4$ pN/nm) (Table 1), the soft linkage via P-selectin-PSGL-1 bond ($k_m \sim 1$ pN/nm) (38) dominates the effective spring constant~ ($k_s \sim k_m$). Here, the stiffer force transducer leads to a higher energetic barrier at a given applied force (37), and the barrier perturbation due to k was corrected by adding an elastic potential into the barrier (19).

Alternatively, when the bond is connected to a soft probe like an OT or BFP transducer, the force transducer would dominate the effective spring constant ($k_s \sim k$). Here, the impact of barrier perturbation due to k on bond dissociation could be neglected since the additional elastic potential is very small. In this study, however, our data indicated that the soft OT probe with low $k \sim 2.5$–30.0×10^{-3} pN/nm (corresponding to $r_f \sim 1$–20 pN/nm) had notable effects on bond dissociation, and the rupture force spectrum still relied on the transducer spring constant used. This finding was in contrast to the existing theory that a low spring constant would not affect the bond rupture (19). One possible interpretation is that very compliant force transducers ($k \ll k_m$) might enable us to readily alter the reactive pathways when a ligand explores the energy landscape presented by a receptor. This could be seen by the fact that rupture forces so measured were significantly

different even at the same loading rate (Fig. 4), suggesting that there exist distinctive reactive pathways for bond dissociation.

Our results indicated that bond dissociation not only depends on loading rate but also relies on mechanical compliance of force transducer when a soft force transducer is used. Although the most probable force was 4.1-fold enhanced when r_f increased from 21 to 188 pN/s (Fig. 6), it was varied with a spring constant but was insensitive to the loading rate at $r_f \leq 20$ pN/s (Fig. 3). These results implied that a high or low spring constant of force transducer has different impacts on bond dissociation. In the case of a high spring constant, i.e., $k \gg k_m$, the energetic barrier height is assumed to increase by $k \times \chi_\beta/2$ when the bond is attached to the transducer, and bond rupture force and reverse rate are enhanced. The effective spring constant k_s remains unchanged, which alters slightly the reactive compliance with increased k (19). In the case of a low spring constant, i.e., $k \ll k_m$, the enhancement in barrier height is limited but the effective spring constant k_s is lowered dramatically, which broadens the reactive compliance with decreased k_s (Table 2). The reactive compliance governs the sensitivity of the energetic landscape to the applied force, which in turn affects the bond rupture forces. High reactive compliance makes the bond dissociation insensitive to applied force, resulting in a loading rate independence of rupture force at low k (Fig. 3 C). Thus, once the bond is mechanically attached to a force transducer, the transducer spring constant (k) introduces an additional barrier height to regulate the reverse rate k_r^0, and the effective spring constant (k_s) governs the variation of barrier width (χ_β) along the reactive pathway.

Bond rupture is synergistically regulated by thermally induced spontaneous dissociation and mechanically mediated forced dissociation, depending on whether the former or the latter dominates the process at different spring constants. Although the work done by applied force, W, at a given temperature is dissipated by extending the trap spring (W_s), lengthening the interacting molecules (W_m), and separating the bond complex (W_c), as well as by resisting the viscous drag (W_v), only the work W_c is effective to force the dissociation of the selectin-ligand bond. To isolate the impact of mechanical tension from that of thermal fluctuation on bond dissociation, we compared the work used to separate the bond complex, W_c, with the thermal energy barrier, $k_B T$, at low and high spring constants. Setting $W_c \sim f^* \times \chi_\beta$ where χ_β is assumed to be ~1 nm (37), the work W_c yields 0.5–1.4 $k_B T$ at $k < 10 \times 10^{-3}$ pN/nm, and 2.3–9.2 $k_B T$ at $k \sim 10.7$–47.0×10^{-3} pN/nm. It is indicated that the impact of thermally induced bond dissociation is comparable to or even more significant than that of mechanically mediated bond dissociation at a low spring constant, whereas it is less significant at a high spring constant (Fig. 3 C).

Another related issue is if laser-induced heating affects bond dissociation during consecutive measurements by enhancing the temperature of the sample pool and fostering Brownian motion of the trapped microbead. We monitored

the temperature of the sample pool around the laser focus and found that it is reasonable to neglect the impact upon the line of reasoning (1): The laser-induced temperature increase ΔT around laser focus is trivial. Using the formulation $\Delta T = (\alpha/2\pi C) \times [\ln(2\pi R/\lambda) - 1] \times P$ where α and C are, respectively, the extinction coefficient and the thermal conductivity of solvent (14.3 m^{-1} and 0.6 W·m^{-1}K^{-1} for water), R the distance of the microbead from the substrate, λ the wavelength of laser, and P the laser power delivered to the sample pool (39), and setting $R \sim 3~\mu$m and $\lambda = 1.064~\mu$m in this study, maximum ΔT was estimated to be $\sim$1 K and $\sim$3 K when P yields $\sim$8–154 and $\sim$262–430 mW (corresponding to spring constant $k \sim (2.5–20.0)$ and $\sim (30.0–47.0) \times 10^{-3}$ pN/nm), respectively (2). The impact of laser-induced heating on spring constant determination using Stokes law is negligible. An empirical formulation was used to estimate the medium viscosity, $\eta(T)$, at absolute temperature, T (40): $\log[\eta(T)] = \{[1.3272 \times (293.15 - T) - 0.001053 \times (293.15 - T)^2]/(T - 168.15) - 2.999\}$. Setting the maximum $\Delta T = 3$ K, the deviation of spring constant determination was $<$6%.

The uncertainty of bond rupture force measurements comes from those for off-center displacement and spring constant determinations. In an off-center displacement measurement, the thermal fluctuation of trapped microbeads varies with the spring constant, and the highest fluctuation at the lowest spring constant yields $\sim$20 nm at a free state (Supplementary Material, Fig. S1 *A*). Noting that the fluctuation is reduced significantly at a bound state without visible rotation and that the most probable off-center displacement is at least one order-of-magnitude higher ($>$400 nm) when the bond dissociates, the uncertainty of the off-center displacement measurement is estimated to be $<$5%. It should be pointed out that an accuracy of 2 nm reported is just the accuracy for the displacement measurement rather than the magnitude of thermal fluctuation. In a spring constant measurement, the accuracy of the measurement depends upon the Stokes formulation, on those for microbead displacement, radius, and velocity at that laser power used. As stated above for a high accuracy of displacement measurement, the uncertainty for the spring constant determination comes mainly from the deviation of laser power. Laser power is controlled to vary 7–430 mW with an accuracy $\leq$1 mW in this study, and the highest deviation of the spring constant at the lowest working laser power yields 6% (Fig. S1 *B*). Taken together, this turns out to be a low uncertainty of the bond rupture force measured (Figs. 3 *C* and 5, *A* and *B*).

It should also be pointed out that elucidating the bond rupture at a low spring constant (and then low loading rates) provides the biophysical bases for understanding the physiological functions of selectin-ligand interactions. Formation, strength, and survival of cell adhesive attachment mediated receptor-ligand interactions depend on how interacting molecules connect to cytostructures beneath the membrane surface (41). Applying adhesion stress via a bond is conceptually like pulling the bond complex using a mechanical spring that mimics the compliant nature of structures attached to the binding site. Thus, stretching the "equivalent" spring produces a force that lowers the chemical activation barrier to increase the frequency of bond dissociation while the spring acts as a force transducer. It has been indicated that, under a pulling force exerted by blood flow, a microvillus is extended (microvillus extension) or a long thin membrane cylinder (tether) is formed which acts like a spring with spring constant $<$0.043 pN/nm. Such a microvillus extension or tether formation lowers the pulling force imposed on the adhesive bonds and thus prolongs the persistence of the bonds at a high physiological shear stress (30). The results presented here indicate that bond dissociation is strongly spring constant dependent at low k (Figs. 3, 5, and 6) compared with those described previously at high k (12–16), which suggests that there might exist a distinctive mechanokinetic mechanism in regulating microvillus extension or tether formation under blood flow.

Finally, we used an OT approach to directly visualize bond dissociation at low spring constants and loading rates. These results demonstrated that the bond rupture is governed mainly by the spring constant, and bond rupture forces present the plateau before a stepwise linear regime with loading rates. This work provides new insights into mapping the bond dissociation of P-selectin-PSGL-1 interactions at low spring constants.

SUPPLEMENTARY MATERIAL

To view all of the supplemental files associated with this article, visit www.biophysj.org.

REFERENCES

1. Lawrence, M. B., and T. A. Springer. 1991. Leukocytes roll on a selectin at physiological flow-rates—distinction from and prerequisite for adhesion through integrins. *Cell.* 65:859–873.

2. McEver, R. P. 2001. Adhesive interactions of leukocytes, platelets, and the vessel wall during hemostasis and inflammation. *Thromb. Haemost.* 86:746–756.

3. McEver, R. P. 2002. Selectins: lectins that initiate cell adhesion under flow. *Curr. Opin. Cell Biol.* 14:581–586.

4. Springer, T. A. 1990. Adhesion receptors of the immune system. *Nature.* 346:425–434.

5. Springer, T. A. 1994. Traffic signals for lymphocyte recirculation and leukocyte emigration—the multistep paradigm. *Cell.* 76:301–314.

6. Vestweber, D., and J. E. Blanks. 1999. Mechanisms that regulate the function of the selectins and their ligands. *Physiol. Rev.* 79:181–213.

7. Ley, K., P. Gaehtgens, C. Fennie, M. S. Singer, L. A. Lasky, and S. D. Rosen. 1991. Lectin-like cell-adhesion molecule-1 mediates leukocyte rolling in mesenteric venules in vivo. *Blood.* 77:2553–2555.

8. Ushiyama, S., T. M. Laue, K. L. Moore, H. P. Erickson, and R. P. Mcever. 1993. Structural and functional-characterization of monomeric soluble P-selectin and comparison with membrane P-selectin. *J. Biol. Chem.* 268:15229–15237.

9. Li, F., H. P. Erickson, J. A. James, K. L. Moore, R. D. Cummings, and R. P. McEver. 1996. Visualization of P-selectin glycoprotein ligand-1 as a highly extended molecule and mapping of protein epitopes for monoclonal antibodies. *J. Biol. Chem.* 271:6342–6348.

10. Moore, K. L., N. L. Stults, S. Diaz, D. F. Smith, R. D. Cummings, A. Varki, and R. P. Mcever. 1992. Identification of a specific glycoprotein ligand for P-selectin (Cd62) on myeloid cells. *J. Cell Biol.* 118:445–456.

11. Bell, G. I. 1978. Models for the specific adhesion of cells to cells. *Science.* 200:618–627.

12. Evans, E., A. Leung, V. Heinrich, and C. Zhu. 2004. Mechanical switching and coupling between two dissociation pathways in a P-selectin adhesion bond. *Proc. Natl. Acad. Sci. USA.* 101:11281–11286.

13. Fritz, J., A. G. Katopodis, F. Kolbinger, and D. Anselmetti. 1998. Force-mediated kinetics of single P-selectin ligand complexes observed by atomic force microscopy. *Proc. Natl. Acad. Sci. USA.* 95:12283–12288.

14. Hanley, W., O. McCarty, S. Jadhav, Y. Tseng, D. Wirtz, and K. Konstantopoulos. 2003. Single molecule characterization of P-selectin/ligand binding. *J. Biol. Chem.* 278:10556–10561.

15. Lü, S. Q., Z. Y. Ye, C. Zhu, and M. Long. 2006. Quantifying the effects of contact duration, loading rate, and approach velocity on P-selectin-PSGL-1 interactions using AFM. *Polymer (Guildf.).* 47:2539–2547.

16. Marshall, B. T., K. K. Sarangapani, J. H. Lou, R. P. McEver, and C. Zhu. 2005. Force history dependence of receptor-ligand dissociation. *Biophys. J.* 88:1458–1466.

17. Rinko, L. J., M. B. Lawrence, and W. H. Guilford. 2004. The molecular mechanics of P- and L-selectin lectin domains binding to PSGL-1. *Biophys. J.* 86:544–554.

18. Marshall, B. T., M. Long, J. W. Piper, T. Yago, R. P. McEver, and C. Zhu. 2003. Direct observation of catch bonds involving cell-adhesion molecules. *Nature.* 423:190–193.

19. Walton, E. B., S. Lee, and K. J. Van Vliet. 2008. Extending Bell's model: how force transducer stiffness alters measured unbinding forces and kinetics of molecular complexes. *Biophys. J.* 94:2621–2630.

20. Evans, E., and K. Ritchie. 1997. Dynamic strength of molecular adhesion bonds. *Biophys. J.* 72:1541–1555.

21. Tees, D. F. J., R. E. Waugh, and D. A. Hammer. 2001. A microcantilever device to assess the effect of force on the lifetime of selectin-carbohydrate bonds. *Biophys. J.* 80:668–682.

22. Alon, R., D. A. Hammer, and T. A. Springer. 1995. Lifetime of the P-selectin-carbohydrate bond and its response to tensile force in hydrodynamic flow. *Nature.* 377:539–542 (Erratum in *Nature* 1995. 376:86).

23. Wuite, G. J. L., R. J. Davenport, A. Rappaport, and C. Bustamante. 2000. An integrated laser trap/flow control video microscope for the study of single biomolecules. *Biophys. J.* 79:1155–1167.

24. Geng, J. G., M. P. Bevilacqua, K. L. Moore, T. M. McIntyre, S. M. Prescott, J. M. Kim, G. A. Bliss, G. A. Zimmerman, and R. P. McEver. 1990. Rapid neutrophil adhesion to activated endothelium mediated by GMP-140. *Nature.* 343:757–760.

25. Moore, K. L., K. D. Patel, R. E. Bruehl, F. G. Li, D. A. Johnson, H. S. Lichenstein, R. D. Cummings, D. F. Bainton, and R. P. Mcever. 1995. P-selectin glycoprotein ligand-1 mediates rolling of human neutrophils on P-selectin. *J. Cell Biol.* 128:661–671.

26. Huang, J., J. Chen, S. E. Chesla, T. Yago, P. Mehta, R. P. McEver, C. Zhu, and M. Long. 2004. Quantifying the effects of molecular orientation and length on two-dimensional receptor-ligand binding kinetics. *J. Biol. Chem.* 279:44915–44923.

27. Wu, L., B. T. Xiao, X. L. Jia, Y. Zhang, S. Q. Lu, J. Chen, and M. Long. 2007. Impact of carrier stiffness and microtopology on two-dimensional kinetics of P-selectin and P-selectin glycoprotein ligand-1 (PSGL-1) interactions. *J. Biol. Chem.* 282:9846–9854.

28. Gelles, J., B. J. Schnapp, and M. P. Sheetz. 1988. Tracking kinesin-driven movements with nanometre-scale precision. *Nature.* 331:450–453.

29. Ghislain, L. P., N. A. Switz, and W. W. Webb. 1994. Measurement of small forces using an optical trap. *Rev. Sci. Instrum.* 65:2762–2768.

30. Shao, J. Y., H. P. Ting-Beall, and R. M. Hochmuth. 1998. Static and dynamic lengths of neutrophil microvilli. *Proc. Natl. Acad. Sci. USA.* 95:6797–6802.

31. Evans, E., A. Leung, D. Hammer, and S. Simon. 2001. Chemically distinct transition states govern rapid dissociation of single L-selectin bonds under force. *Proc. Natl. Acad. Sci. USA.* 98:3784–3789.

32. Tees, D. F. J., J. T. Woodward, and D. A. Hammer. 2001. Reliability theory for receptor-ligand bond dissociation. *J. Chem. Phys.* 114:7483–7496.

33. Chesla, S. E., P. Selvaraj, and C. Zhu. 1998. Measuring two-dimensional receptor-ligand binding kinetics by micropipette. *Biophys. J.* 75:1553–1572.

34. Long, M., H. Zhao, K. S. Huang, and C. Zhu. 2001. Kinetic measurements of cell surface E-selectin/carbohydrate ligand interactions. *Ann. Biomed. Eng.* 29:935–946.

35. Zhu, C., M. Long, S. E. Chesla, and P. Bongrand. 2002. Measuring receptor/ligand interaction at the single-bond level: experimental and interpretative issues. *Ann. Biomed. Eng.* 30:305–314.

36. Evans, E. 2001. Probing the relation between force—lifetime—and chemistry in single molecular bonds. *Annu. Rev. Biophys. Biomol. Struct.* 30:105–128.

37. Sarangapani, K. K., T. Yago, A. G. Klopocki, M. B. Lawrence, C. B. Fieger, S. D. Rosen, R. P. McEver, and C. Zhu. 2004. Low force decelerates L-selectin dissociation from P-selectin glycoprotein ligand-1 and endoglycan. *J. Biol. Chem.* 279:2291–2298.

38. Marshall, B. T., K. K. Sarangapani, J. H. Wu, M. B. Lawrence, R. P. McEver, and C. Zhu. 2006. Measuring molecular elasticity by atomic force microscope cantilever fluctuations. *Biophys. J.* 90:681–692.

39. Peterman, E. J. G., F. Gittes, and C. F. Schmidt. 2003. Laser-induced heating in optical traps. *Biophys. J.* 84:1308–1316.

40. Weast, R. C., editor. 1973. CRC Handbook of Chemistry and Physics, 53rd ed. CRC Press, Boca Raton, FL.

41. Evans, E. A., and D. A. Calderwood. 2007. Forces and bond dynamics in cell adhesion. *Science.* 316:1148–1153.